ACS APPLIED MATERIALS & INTERFACES

Research Article

www.acsami.org

Layered Na_xMnO_{2+z} in Sodium Ion Batteries—Influence of Morphology on Cycle Performance

Nicolas Bucher,[∥,†,‡] Steffen Hartung,[∥,†,‡] Arun Nagasubramanian,[†,§] Yan Ling Cheah,[§] Harry E. Hoster,[†,‡] and Srinivasan Madhavi*[,†,§]

[†]TUM CRREATE, Singapore 138602, Singapore

[‡]Technische Universität München, 85748 Garching, Germany

[§]School of Materials Science and Engineering, Nanyang Technological University, Singapore 639798, Singapore

Supporting Information

ABSTRACT: Due to its potential cost advantage, sodium ion batteries could become a commercial alternative to lithium ion batteries. One promising cathode material for this type of battery is layered sodium manganese oxide. In this investigation we report on the influence of morphology on cycle performance for the layered Na_xMnO_{2+z}. Hollow spheres of Na_xMnO_{2+z} with a diameter of ∼5 μm were compared to flake-like Na_xMnO_{2+z}. It was found that the electrochemical behavior of both materials as measured by cyclic voltammetry is comparable. However, the cycle stability of the spheres is significantly higher, with 94 mA h g^{-1} discharge capacity after 100 cycles, as opposed to 73 mA h g^{-1} for the flakes (50 mA g^{-1}). The better stability can potentially be attributed to better accommodation of volume changes of the material due to its spherical morphology, better contact with the added conductive carbon, and higher electrode/electrolyte interface owing to better wetting of the active material with the electrolyte.

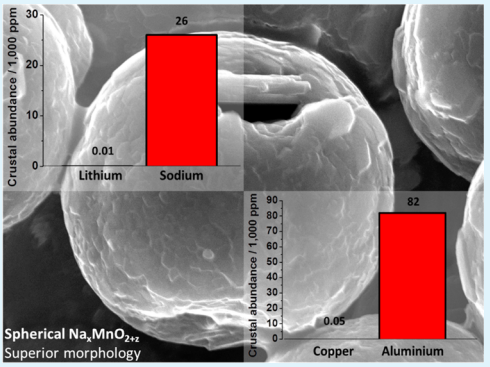

KEYWORDS: *sodium ion battery, energy storage, sodium manganese oxide, spheres, morphology*

1. INTRODUCTION

Electrochemical energy storage technologies have become an important field of research, as the need to flexibly store electricity has greatly increased over the last years. This can be seen in a variety of areas in everyday life, from portable consumer electronics like laptops and smartphones, electrically powered vehicle to boost electro mobility, to the need of large-scale energy storage to smoothen erratic fluctuations of electricity generated by renewable sources.

Over the last years and decades, the intercalation-based lithium ion battery (LIB) technology has been at the centre of this research, due to its high power density and capacity. However, as the necessity for flexible and affordable energy storage pervades more and more areas, relying on this technology might pose several problems. First, with a crustal abundance of 10 ppm,[1] lithium resources are limited, and hence, it is uncertain whether these resources can sustain a considerably elevated demand. Moreover, as LIBs are already a relatively expensive technology, a significantly higher demand could increase prices even further. Therefore, research has recently also focused on alternative energy storage technologies. One promising candidate is sodium ion batteries (NIB). NIB is based on the same working principle as LIB but uses sodium as the electroactive species.[2−7] With a crustal abundance of sodium of 26 000 ppm, (see abstract graphic)[1] both availability and price make NIB a promising option to complement (or even eventually replace) LIB in certain areas. Furthermore, in contrast to LIB which uses copper as anode current collector, NIB can use the cheaper and more abundant Al, as it does not alloy with Na.[8−10] However, one inherent disadvantage is that sodium compounds usually provide lower performance. Several classes of cathode materials have been studied in the field of NIB. $NaFePO_4$ provides a high cycle stability and acceptable capacity.[11] Different (sodium) vanadium oxides were studied and show promising performances. NaV_6O_{15}, for example, provides 142 mA h g^{-1}, and NaV_3O_8 delivers a capacity of 200 mA h g^{-1}.[12−17] Jian et al. recently showed that $Na_3V_2(PO_4)_3$ is a promising material,[18] and Xu et al. published a study on $Na_3V_2O_2(PO_4)_2F$/graphene, which shows a high intercalation potential (>3.5 V), combined with a good capacity and stability.[19] Layered oxides are among the most promising materials to deliver the performance required for practical applications.[20−31] Vassilaras et al., for example, recently reported approximately 160 mA h g^{-1} for $NaNi_{1/3}Co_{1/3}Fe_{1/3}O_2$,[32] and Wang et. al. published a work of $Na_{0.66}[Li_{0.22}Ti_{0.78}]O_2$ as an anode material with a low volume change, in which they also studied the position of Na in the interlayer.[33] Within this class of materials, sodium manganese

Received: December 27, 2013
Accepted: May 12, 2014
Published: May 12, 2014

   dx.doi.org/10.1021/am406009t | ACS Appl. Mater. Interfaces 2014, 6, 8059−8065

based oxides have received special attention, as manganese is relatively abundant.[1] Furthermore, these compounds have shown that they are able to deliver considerable capacities.[34−37]

Various attempts have been made to improve specific characteristics (e.g., cycle stability) by partially substituting manganese with other transition metals like Co, Ni, or Fe.[10,37−39] Yabuuchi et al., for example, reported good capacities and stabilities for $Na_xFe_{1/2}Mn_{1/2}O_2$.[10]

A different approach to decrease capacity fading is optimization of the morphology. Hollow spherical nanostructured morphologies possess favorable characteristics such as high surface-to-volume ratio, low density and low coefficients of thermal expansion as compared to their bulk micrometer sized counterparts. For example it has been shown that for $LiNi_{0.5}Mn_{1.5}O_4$, $LiMn_2O_4$, and $ZnMn_2O_4$ spherical particles considerably enhance cycle stability in LIB applications.[40−43]

In this publication, we demonstrate that this approach is beneficial in the field of sodium ion batteries, in general, and sodium manganese oxides in particular. For this purpose, we will first describe the synthesis of spherical sodium manganese oxides along with physical characterization studies such as X-ray diffraction (XRD), scanning electron microscopy (SEM), and transmission electron microscopy (TEM).We have evaluated the electrochemical performance of this material and compared it to a sodium manganese oxide that has been synthesized through a different route, which yielded a flake-like morphology. We present in this work the effect of morphology on the electrochemical performance of sodium manganese oxide (NMO) in sodium ion batteries.

2. EXPERIMENTAL SECTION

2.1. Synthesis. Spherical NMO was synthesized using spherical MnO_2 as precursor, which was synthesized according to a slightly modified procedure described by Li et al.[44] Spherical MnO_2 was synthesized by first dissolving NH_4HCO_3 in deionized water. Then, a small amount of ethanol (10% volume of the NH_4HCO_3 solution) and a solution of $MnSO_4$ in deionized water was added dropwisely. During the subsequent stirring at room temperature, spherical $MnCO_3$ was forming. The precipitate was filtrated, washed repeatedly with water and ethanol, and afterwards annealed in air for 5 h at 400 °C to give spherical MnO_2. Next, this was added to a solution of NaOH in deionized water and ethanol to give a dispersion. Both water and ethanol were evaporated, and the residue was annealed in air for 3 h at 320 °C, followed by 4 h at 800 °C to give the targeted spherical sodium manganese oxide.

Flake-like NMO was synthesized as described previously by our group.[37] Sodium nitrate (Sigma-Aldrich, ≥99%), manganese acetate (Alfa Aesar, anhydrous, 98%), and gelatin were dissolved in deionized water and nitric acid (≥69%, Honeywell). The solution was heated to 250 °C until spontaneous combustion set in. Subsequently, the product was annealed in air for 4 h at 800 °C to give the flake-like NMO.

2.2. Characterization. The crystal structures of the products were verified by powder X-ray diffraction, using a Bruker X-ray diffractometer with Cu Kα radiation. 2θ was varied within a range of $10° < 2\theta < 80°$, using a step size of 0.02° and 0.9 s per step. The Topas software (version 3) was used to conduct a phase analysis. The product morphologies were analysed by field emission scanning electron microscopy (FESEM, JEOL JSM-7600F) and transmission electron microscopy (TEM, JEOL 2100F, 200 kV). Elemental compositions were determined by micro X-ray fluorescence analysis (XRF, Bruker/M4 Tornado), using Rh as X-ray source (50 kV, 200 μm).

2.3. Electrochemistry. The composite electrodes were prepared by mixing NMO with acetylene black (Alfa Aesar, > 99%) and polyvinylidene fluoride (PVDF, Arkema, Kynar HSV 900) binder in the weight ratio 60:20:20 with *N*-methyl-2-pyrrolidone (NMP) to form a homogeneous slurry. This mixture was coated on an Al foil using a doctor blade; the coating was dried in air at 80 °C to remove the NMP. The coating was punched into pieces with a diameter of 16 mm, which were then roll-pressed, so that the electrodes prepared from flake-like and spherical NMO had comparable packing densities. Subsequently, they were dried at 110 °C under vacuum. These electrodes were then assembled in 2016 coin cells with circular metallic sodium pieces with a diameter of 16 mm as the anode, and glass fibre (Whatman) as the separator. A 1M solution of $NaClO_4$ (Sigma-Aldrich, ≥98%) in a mixture of ethylene carbonate and propylene carbonate (1:1 wt %; EC, Sigma-Aldrich, 99%; PC, Sigma-Aldrich, ≥99.7%) was employed as electrolyte. Cyclic voltammetry was measured using a BioLogic potentiostat, and a Neware battery tester was used for galvanostatic charge/discharge tests.

3. RESULTS

3.1. Morphology and Structure. Spherical MnO_2 (Figure 1a and b) was synthesized as a precursor for spherical NMO. The MnO_2 spheres are approximately 5 μm in diameter and

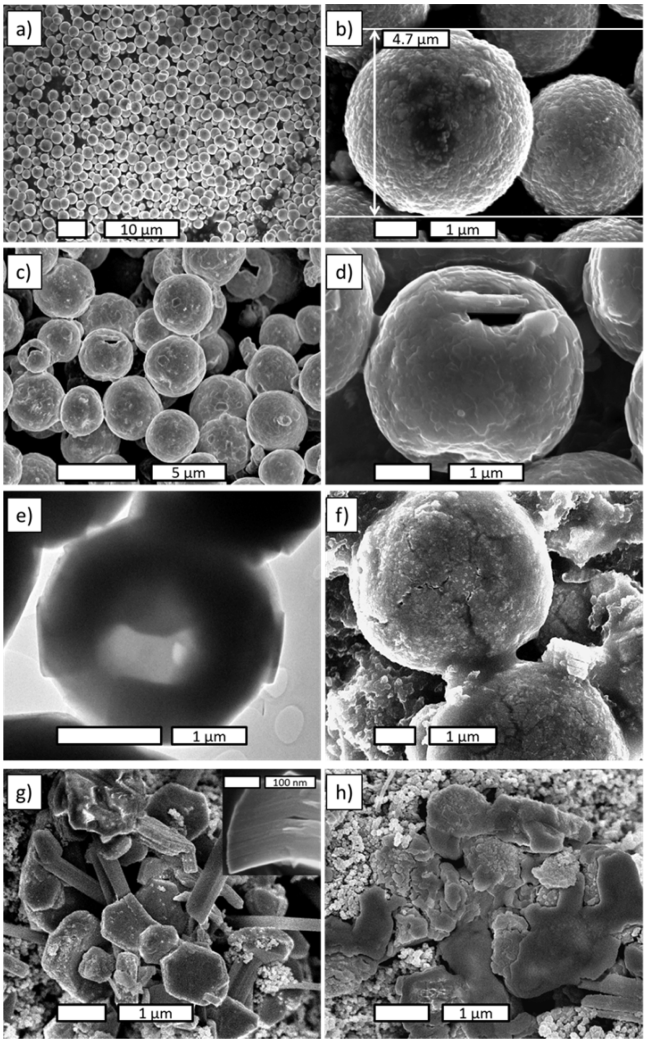

Figure 1. (a and b) SEM image of spherical MnO_2, (c and d) SEM image of spherical NMO, (e) TEM image of spherical NMO, (f) SEM image of a spherical NMO electrode after 100 cycles, surrounded by PVDF binder and acetylene black, (g) SEM image of flake-like NMO electrode before cycling, (h) SEM image of a flake-like NMO electrode after 100 cycles, surrounded by PVDF binder and acetylene black.

consist of fused, cubic crystallites. Sodium manganese oxide maintains this morphology (Figure 1c). However, during the synthesis process, some of the spheres seem to have opened up. Thus, a cross-section became visible (Figure 1d), indicating that the spheres are hollow, and that the shells are composed of sodium manganese layers with a thickness of several hundred nanometers. TEM pictures (Figure 1e) confirm that the spheres are hollow. Moreover, they indicate polycrystallinity of the material. After 100 cycles, the morphology is maintained (Figure 1f). Although minor cracks are visible, the spheres are preserved. The flakes, however, do not maintain their initial morphology. Figure 1g shows flake-like NMO on an electrode; after 100 cycles (Figure 1h), the flakes appear degraded and fused, indicating that morphology is degrading during cycling. The flake-like NMO shows the same morphology as described previously, that is, layered flakes with a cross-section of several hundred nanometers (see inset in Figure 1g).[37] BET measurements showed a comparable surface area of approximately 5 m^2 g^{-1}. However, the macropores in the spheres (Figure 1d, e) can contribute to better wetting of the active material with electrolyte.

For both morphologies, NMO was synthesized in the layered P2 structure (space group $P6_3mmc$). The crystal structure consists of layers of MnO_6 octahedra, while the sodium ions occupy two different triangular prismatic sides in between these layers. This was confirmed by XRD measurements (Figure 2).

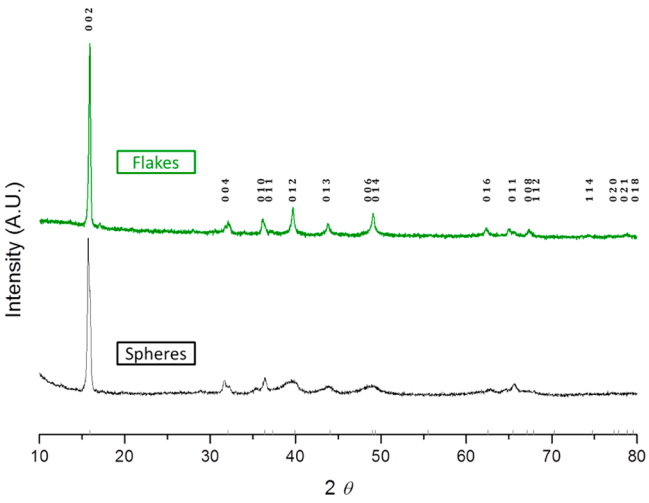

Figure 2. XRD pattern of the flake-like and spherical NMO.

The patterns for layered and spherical NMO, which were synthesized via similar annealing procedures, show that both materials have the same phase, albeit the flakes are more crystalline than the spheres. The crystallite size of the flakes, as estimated by the Debye–Scherer equation on the peak half maximum for different peaks, exceeds the crystallite size of the spheres (22–36 nm vs 4–20 nm). P2-type sodium manganese oxide occurs in the α and the β form. The XRD pattern of the synthesized spherical material corresponds to the α form; the additional small impurity peak at $2\theta = 32°$ can be attributed to the β form. As the oxygen content slightly varies for these two different forms, we write the chemical formula as Na_xMnO_{2+z}, with $0 \leq z \leq 0.25$.[45] XRF measurements showed that, initially, $x = 0.8$ for the spheres, and $x = 0.6$ for the flakes. The unit cell volume changes, according to Patoux et al., by approximately 1% upon (de-)insertion of 0.1 Na.[46]

3.2. Electrochemistry. Figure 3d shows the cyclic voltammogram (CV) of spherical NMO at a scan rate of 0.1 mV s^{-1}, which is remarkably similar to the CV of the layered NMO discussed earlier.[37] The main oxidation peak occurs around 2.45 V, and the corresponding reduction peak around 2.22 V. At higher voltages, several oxidation and reduction peaks are visible, which can mainly be attributed to phase transitions due to ordering process of the sodium ions between the two different triangular prismatic sites.

In the cycling profile of spherical NMO for 50 mA g^{-1}, as can be seen in Figure 3a, the significant peaks that can be seen in the CV can be observed as well. The dominating feature is the plateau around 2.3 V. As the half-cell is charged first, a certain amount of sodium is removed from the NMO structure. The observed capacity in the first charge is 47 mA h g^{-1}, which corresponds to 0.27 Na^+ per formula unit. The structure of this material varies with its sodium content—from the structure at hand, Na^+ can be removed until a stoichiometry of ca. $Na_{0.44}$ is reached.[45] Thus, in the first charge Na^+ can potentially be removed from the structure with the initial composition only until this barrier, which is why the capacity is rather low. Upon discharge, the structure is filled with sodium, which is removed in subsequent charge cycles. Thus, subsequent charge capacities are considerably higher. The first discharge capacity is 161 mA h g^{-1}, which decreases to 120 mA h g^{-1} after 50, and 94 mA h g^{-1} after 100 cycles.

Flake-like NMO shows a slightly lower capacity for both initial charge (34 mA h g^{-1}) and discharge (140 mA h g^{-1}) as compared to the spherical NMO. These values for initial discharge capacities for both spherical and flake-like NMO are comparable to previously reported capacities of layered oxides.[35,37,39] The initial charge capacity of the NMO flakes is slightly decreased as compared to our previous work,[37] which hints at a lower initial sodium content. However, as the (de-)insertion of Na^+ is reversible, this difference should be compensated upon the first charge. Similarly, as both the spheres and the flakes were first charged, a common baseline is created as all the sodium that can be deinserted from this P2 structure in this voltage range is removed, so that after the first charge the Na-content for spheres and flakes should be similar. For our experiments, the electrolyte used was a mixture of ethylene carbonate and propylene carbonate (1:1 wt %), which resulted in a better cycle stability as compared to the previously reported electrolyte without ethylene carbonate. For the flakes, a discharge capacity of 87 mA h g^{-1} was observed after 50 cycles, and 73 mA h g^{-1} after 100 cycles (see Figure 4). After 20 cycles, a capacity of 105 mA h g^{-1} can be achieved, which indicates a better stability than previously reported NMO.[37] This can probably be attributed to the addition of ethylene carbonate to the electrolyte.[47−49]

However, a significant difference in cycle stability can be seen between the spherical and the flake-like NMO, with the spheres providing 120 mA h g^{-1} after 50 cycles as opposed to 87 mA h g^{-1} for the flakes, and 94 mA h g^{-1} as compared to 73 mA h g^{-1} after 100 cycles, respectively (Figure 4). Thus, a higher capacity can be maintained for the spherical morphology.

Moreover, more pronounced plateaux at higher voltages (i.e., above 2.3 V) were observed when changing the morphology from flake-like to spherical (Figure 3b). Thus, it seems that transformations occurring at these voltages can be better addressed and exploited with hollow spheres. As can be seen in the direct comparison of the cyclic voltammograms of spherical and flake-like NMO (0.1 mV s^{-1}, Figure 3d), both materials

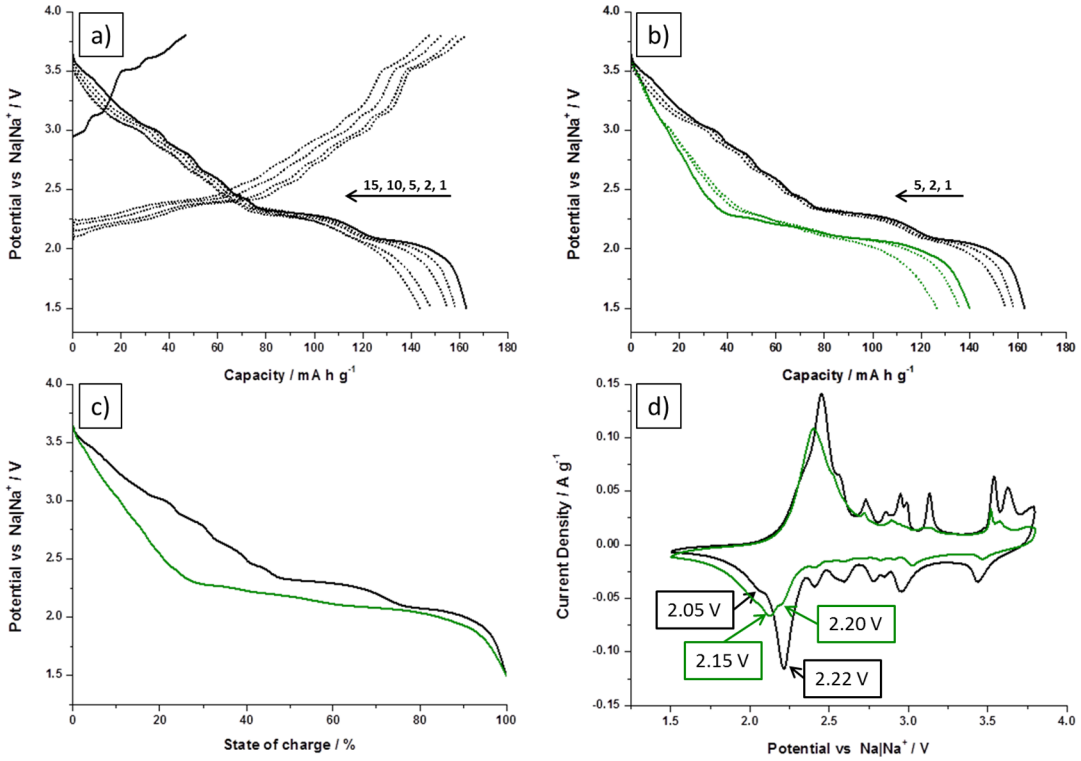

Figure 3. (a) Charge/discharge profile of spherical NMO at 50 mA g^{-1}; half-cell vs Na in 1 M $NaClO_4$ in propylene carbonate/ethylene carbonate (1:1 wt %); (b) discharge profile of spherical (black) and flake-like (green) NMO at 50 mA g^{-1}; (c) state of discharge profile of spherical (black) and flake-like (green) NMO, (d) cyclic voltammogram of spherical (black) and flake-like (green) NMO at 0.1 mV s^{-1}.

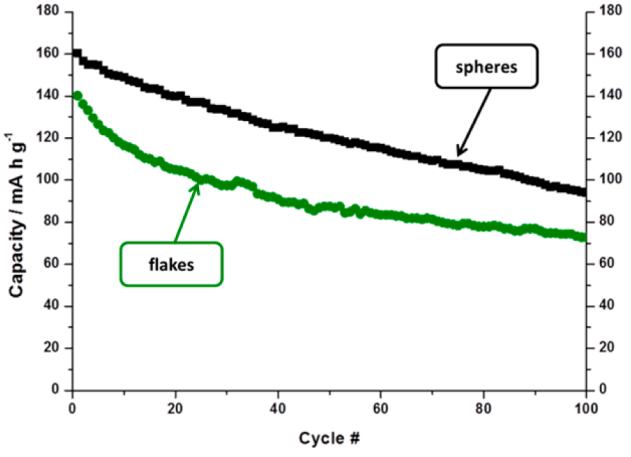

Figure 4. Cycling behavior of NMO at 50 mA g^{-1}; black, spherical; green, flake-like.

exhibit the same peaks, although they are significantly more pronounced for the hollow spheres, which corresponds to the discharge profiles. Thus, similar redox reactions, phase transformations or ordering processes occur in both materials; they are not suppressed in the flake-like material. An interesting feature in these CVs is that for the hollow spheres, the main reduction peak occurs at 2.22 V with a small shoulder peak at 2.05 V, whereas for the flakes the main peak is at 2.15 V with a small shoulder peak at 2.20 V. Even though a small shift can be attributed to polarization effects, it is noticeable that the peak intensity seem to have switched: a main peak with a shoulder at a higher voltage for the flakes, and a shoulder peak with a main peak at a higher voltage for the spheres.

This, together with the increased total capacity, results in an increase in energy density. The energy density was increased from 322 W h kg^{-1} (flakes) to 408 W h kg^{-1} (spheres), which corresponds to an increase of 27%. When normalized to state of discharge (Figure 3c), it can be seen that this increase is to a large extend (34%) attributable to a better exploitation of insertion processes, resulting in increased capacity for these processes.

Moreover, the hollow spheres also show remarkable capacities at higher current rates (Figure 5). Although the initial capacities decrease with increasing current rate, capacities seem to converge after 100 cycles. Therefore, this material is well suitable for applications for which fast discharge is

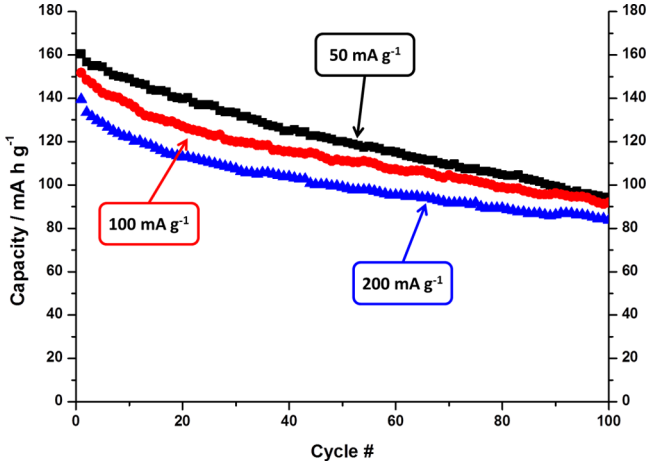

Figure 5. Cycling behavior of spherical NMO at different current rates.

dx.doi.org/10.1021/am406009t | ACS Appl. Mater. Interfaces 2014, 6, 8059−8065

necessary. The influence of current rate on capacity can be seen in Figure 6 for both flake-like and spherical NMO.

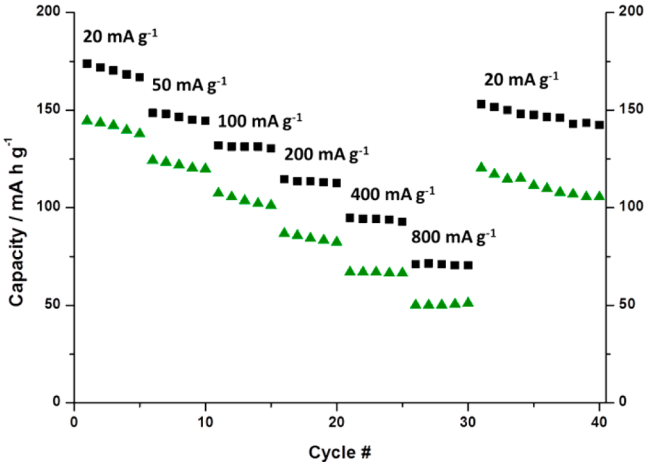

Figure 6. Cycling behavior of NMO; black (upper curve), spherical; green (lower curve), flake-like.

This conclusion that hollow spheres exhibit a higher cycle stability than other morphologies has also been found for materials of other chemical compositions.[41−43] Several arguments for this behavior have been introduced. First, hollow spheres can more easily accommodate the volume change that is inherently caused by the (de-)insertion of lithium or sodium into (from) the host structure. Thus, morphology is maintained over a longer time, resulting in higher cycle stability. Especially for sodium (de-)insertion, which distorts the structure to an even greater extent, this characteristic is highly significant. This assumption has been verified by opening a cell that had been cycled for 100 cycles at 200 mA g^{-1} and examining the morphology. As can be seen from Figure 1f, the spherical morphology is retained throughout cycling Thus, the inherent advantages of this morphology are retained as well. Moreover, as opposed to bulk materials, hollow spheres distinguish themselves through singular particles with defined boundaries, which enhances uniform mixing with the added conductive carbon. This could lead to a longer-lasting contact between the active material and the necessary conductive carbon, resulting in better cycle stability. Another effect is that the electrolyte penetration is enhanced, and thus, the diffusion pathway for sodium ions is shortened. Better crystallinity can be ruled out as a potential factor for the superior performance of the spheres as crystallinity is higher for the flakes (see section 3.1). As shown previously, cycle stability can potentially be improved even further by partially substituting manganese with other metals, such as cobalt.[37]

4. CONCLUSION

Different synthesis routes that yield different morphologies of sodium manganese oxide were explored. Specifically, flake-like and spherical sodium manganese oxide with the same P2-type crystal structure were obtained. Both materials show the same electrochemical behavior as measured by cyclic voltammetry, while the spheres provide slightly higher discharge capacities (140 vs 161 mA h g^{-1}, respectively) for a current rate of 50 mA g^{-1}. After 100 cycles, a higher discharge capacity could be maintained for the hollow spheres (94 mA h g^{-1} as opposed to 73 mA h g^{-1}). Moreover, energy density could be increased by 27%, due to an increase in capacity, especially based on more pronounced plateaux at higher voltage regions. As both materials have been tested under the same conditions, it can safely be assumed that the spherical morphology is responsible for the increase in cyclability, probably due to better accommodation of volume changes, better contact with the conductive carbon, and shortened sodium ion diffusion pathways. Even for higher current rates, spherical NMO shows remarkable cycle stability so that, for example, after 100 cycles, 84 mA h g^{-1} can still be achieved for 200 mA g^{-1}.

Therefore, we have proven that a change in morphology towards spheres does not only work for LIB systems but also for sodium ion batteries. Moreover, we have demonstrated that spherical, P2-type NMO is a suitable sodium ion battery cathode material for applications that require high capacities and cycle stability.

■ ASSOCIATED CONTENT

Ⓢ Supporting Information

Figure S1 shows the (ex-situ) XRD of the flake-like and spherical NMO after cycling, indicating that the main structure is largely maintained and small transformations occur for both materials. The impurity peak at $2\theta = 13$ can be attributed to the birnessite structure, which was probably formed while handling the sample in atmosphere. Figure S2 shows SEM images of the flake-like NMO after cycling to substantiate the claim that the particles that can be seen in Fig. 1h are indeed NMO. This material is available free of charge via the Internet at http://pubs.acs.org/.

■ AUTHOR INFORMATION

Corresponding Author

*Email: Madhavi@ntu.edu.sg.

Author Contributions

∥The manuscript was written through contributions of all authors. All authors have given approval to the final version of the manuscript. N.B. and S.H. contributed equally to this manuscript.

Funding

This work was financially supported by the Singapore National Research Foundation under its Campus for Research Excellence and Technological Enterprise (CREATE) programme.

Notes

The authors declare no competing financial interest.

■ ACKNOWLEDGMENTS

Y.L.C. acknowledges the World Future Foundation for their support.

■ REFERENCES

(1) Mp, X. *Springer Materials* (www.springermaterials.com) Landolt-Boernstein Databaset-Boernstein Database; Springer: New York; pp 248−250, 1984.

(2) Ellis, B. L.; Nazar, L. F. Sodium and Sodium-Ion Energy Storage Batteries. *Curr. Opin. Solid State Mater. Sci.* **2012**, *16*, 168−177.

(3) Palomares, V.; Serras, P.; Villaluenga, I.; Hueso, K. B.; Carretero-González, J.; Rojo, T. Na-Ion Batteries, Recent Advances and Present Challenges to Become Low Cost Energy Storage Systems. *Energy Environ. Sci.* **2012**, *5*, 5884−5901.

(4) Palomares, V.; Casas-Cabanas, M.; Castillo-Martínez, E.; Han, M. H.; Rojo, T. Update on Na-Based Battery Materials. A Growing Research Path. *Energy Environ. Sci.* **2013**, *6*, 2312−2337.

(5) Kim, S.-W.; Seo, D.-H.; Ma, X.; Ceder, G.; Kang, K. Electrode Materials for Rechargeable Sodium-Ion Batteries: Potential Alternatives to Current Lithium-Ion Batteries. *Adv. Energy Mater.* **2012**, *2*, 710−721.
(6) Chevrier, V. L.; Ceder, G. Challenges for Na-Ion Negative Electrodes. *J. Electrochem. Soc.* **2011**, *158*, A1011−A1014.
(7) Pan, H.; Hu, Y.-S.; Chen, L. Room-Temperature Stationary Sodium-Ion Batteries for Large-Scale Electric Energy Storage. *Energy Environ. Sci.* **2013**, *6*, 2338−2360.
(8) Komaba, S.; Murata, W.; Ishikawa, T.; Yabuuchi, N.; Ozeki, T.; Nakayama, T.; Ogata, A.; Gotoh, K.; Fujiwara, K. Electrochemical Na Insertion and Solid Electrolyte Interphase for Hard-Carbon Electrodes and Application to Na-Ion Batteries. *Adv. Funct. Mater.* **2011**, *21*, 3859−3867.
(9) Komaba, S.; Ishikawa, T.; Yabuuchi, N.; Murata, W.; Ito, A.; Ohsawa, Y. Fluorinated Ethylene Carbonate as Electrolyte Additive for Rechargeable Na Batteries. *ACS Appl. Mater. Interfaces* **2011**, *3*, 4165−4168.
(10) Yabuuchi, N.; Kajiyama, M.; Iwatate, J.; Nishikawa, H.; Hitomi, S.; Okuyama, R.; Usui, R.; Yamada, Y.; Komaba, S. P2-Type $Na_x[Fe_{1/2}Mn_{1/2}]O_2$ Made from Earth-Abundant Elements for Rechargeable Na Batteries. *Nat. Mater.* **2012**, *11*, 512−517.
(11) Oh, S.-M.; Myung, S.-T.; Hassoun, J.; Scrosati, B.; Sun, Y.-K. Reversible $NaFePO_4$ Electrode for Sodium Secondary Batteries. *Electrochem. Commun.* **2012**, *22*, 149−152.
(12) Liu, H.; Zhou, H.; Chen, L.; Tang, Z.; Yang, W. Electrochemical Insertion/Deinsertion of Sodium on NaV_6O_{15} Nanorods as Cathode Material of Rechargeable Sodium-Based Batteries. *J. Power Sources* **2011**, *196*, 814−819.
(13) Novak, P.; Scheifele, W.; Haas, O. Magnesium Insertion Batteries - an Alternative to Lithium? *J. Power Sources* **1995**, *54*, 479−482.
(14) West, K.; Zachau-Christiansen, B.; Jacobsen, T.; Jacobsen, T. Sodium Insertion in Vanadium Oxides. *Solid State Ionics* **1988**, *28-30*, 1128−1131.
(15) Wang, G.; Pistoia, G. Rechargeable All Solid-State Lithium and Sodium Cells with Composite Cathodic Films Based on $Na_{1+x}V_3O_8$. *J. Electroanal. Chem.* **1991**, *302*, 275−278.
(16) He, H.; Jin, G.; Wang, H.-Y.; Huang, X.; Chen, Z.; Sun, D.; Tang, Y.-G. Annealed NaV_3O_8 Nanowires with Good Cycling Stability as a Novel Cathode for Na-Ion Battery. *J. Mater. Chem. A* **2013**, *2*, 3563−3570.
(17) Hartung, S.; Bucher, N.; Nair, V. S.; Ling, C. Y.; Wang, Y.; Hoster, H. E.; Srinivasan, M. Sodium Vanadium Oxide − a New Material for High-Performance Symmetric Sodium Ion Batteries. *Chem. Phys. Chem.* **2014**, 10.1002/cphc.201402020R1.
(18) Jian, Z.; Han, W.; Lu, X.; Yang, H.; Hu, Y.-S.; Zhou, J.; Zhou, Z.; Li, J.; Chen, W.; Chen, D.; Chen, L. Superior Electrochemical Performance and Storage Mechanism of $Na_3V_2(PO_4)_3$ Cathode for Room-Temperature Sodium-Ion Batteries. *Adv. Energy Mater.* **2013**, *3*, 156−160.
(19) Xu, M.; Wang, L.; Zhao, X.; Song, J.; Xie, H.; Lu, Y.; Goodenough, J. B. $Na_3V_2O_2(PO_4)_2F$/Graphene Sandwich Structure for High-Performance Cathode of a Sodium-Ion Battery. *Phys. Chem. Chem. Phys.* **2013**, *15*, 13032−13037.
(20) Berthelot, R.; Carlier, D.; Delmas, C. Electrochemical Investigation of the P2−Na_xCoO_2 Phase Diagram. *Nat. Mater.* **2011**, *10*, 74−80.
(21) Bhide, A.; Hariharan, K. Physicochemical Properties of Na_xCoO_2 as a Cathode for Solid State Sodium Battery. *Solid State Ionics* **2011**, *192*, 360−363.
(22) Braconnier, J. J.; Delmas, C.; Hagenmuller, P. Etude par Desintercalation Electrochimique des Systemes Na_xCrO_2 et Na_xNiO_2. *Mater. Res. Bull.* **1982**, *17*, 993−1000.
(23) D'Arienzo, M.; Ruffo, R.; Scotti, R.; Morazzoni, F.; Mari, C. M.; Polizzi, S. Layered $Na_{0.71}CoO_2$: A Powerful Candidate for Viable and High Performance Na-Batteries. *Phys. Chem. Chem. Phys.* **2012**, *14*, 5945−5952.
(24) Ding, J. J.; Zhou, Y. N.; Sun, Q.; Yu, X. Q.; Yang, X. Q.; Fu, Z. W. Electrochemical Properties of P2-phase $Na_{0.74}CoO_2$ Compounds as Cathode Material for Rechargeable Sodium-Ion Batteries. *Electrochim. Acta* **2013**, *87*, 388−393.
(25) Guignard, M.; Didier, C.; Darriet, J.; Bordet, P.; Elkaïm, E.; Delmas, C. P2-Na_xVO_2 System as Electrodes for Batteries and Electron-Correlated Materials. *Nat. Mater.* **2012**, *11*, 1−7.
(26) Meng, Y. S.; Hinuma, Y.; Ceder, G. An Investigation of the Sodium Patterning in Na_xCoO_2 ($0.5 < \text{or} = x < \text{or} = 1$) by Density Functional Theory Methods. *J. Chem. Phys.* **2008**, *128*, 104708-1−104708-8.
(27) Shu, G.; Prodi, A.; Chu, S.; Lee, Y.; Sheu, H.; Chou, F. Searching for Stable Na-Ordered Phases in Single-Crystal Samples of γ-Na_xCoO_2. *Phys. Rev. B* **2007**, *76*, 184115-1−184115-9.
(28) Takahashi, Y.; Akimoto, J.; Kijima, N.; Gotoh, Y. Structure and Electron Density Analysis of $Na_{0.74}CoO_2$ by Single-Crystal X-ray Diffraction. *Solid State Ionics* **2004**, *172*, 505−508.
(29) Xia, X.; Dahn, J. R. A Study of the Reactivity of De-Intercalated P2-Na_xCoO_2 with Nonaqueous Solvent and Electrolyte by Accelerating Rate Calorimetry. *J. Electrochem. Soc.* **2012**, *159*, A647−A650.
(30) Zandbergen, H.; Foo, M.; Xu, Q.; Kumar, V.; Cava, R. Sodium Ion Ordering in Na_xCoO_2: Electron Diffraction Study. *Phys. Rev. B* **2004**, *70*, 024101-1−024101-8.
(31) Zhang, P.; Capaz, R.; Cohen, M.; Louie, S. Theory of Sodium Ordering in Na_xCoO_2. *Phys. Rev. B: Condens. Matter* **2005**, *71*, 153102-1−153102-4.
(32) Vassilaras, P.; Toumar, A. J.; Ceder, G. Electrochemical Properties of $NaNi_{1/3}Co_{1/3}Fe_{1/3}O_2$ as a Cathode Material for Na-Ion Batteries. *Electrochem. Commun.* **2014**, *38*, 79−81.
(33) Wang, Y.; Yu, X.; Xu, S.; Bai, J.; Xiao, R.; Hu, Y.-S.; Li, H.; Yang, X.-Q.; Chen, L.; Huang, X. A Zero-Strain Layered Metal Oxide as the Negative Electrode for Long-Life Sodium-Ion Batteries. *Nat. Commun.* **2013**, *4*, 2365.
(34) Wu, F.; Yu, G.; Xu, D.; Kan, E. First-Principles Investigations on the Magnetic Structure of α-$NaMnO_2$. *J. Phys.: Condens. Matter* **2012**, *24*, 456002-1−456002-5.
(35) Caballero, A.; Hernán, L.; Morales, J.; Sánchez, L.; Santos, J. Ion-Exchange Properties of P2-Na_xMnO_2: Evidence of the Retention of the Layer Structure Based on Chemical Reactivity Data and Electrochemical Measurements of Lithium Cells. *J. Solid State Chem.* **2003**, *174*, 365−371.
(36) Ma, X.; Chen, H.; Ceder, G. Electrochemical Properties of Monoclinic $NaMnO_2$. *J. Electrochem. Soc.* **2011**, *158*, A1307−A1312.
(37) Bucher, N.; Hartung, S.; Gocheva, I.; Cheah, Y. L.; Srinivasan, M.; Hoster, H. E. Combustion-Synthesized Sodium Manganese (Cobalt) Oxides as Cathodes for Sodium Ion Batteries. *J. Solid State Electrochem.* **2013**, *17*, 1923−1929.
(38) Kim, D.; Lee, E.; Slater, M.; Lu, W.; Rood, S.; Johnson, C. S. Layered $Na[Ni_{1/3}Fe_{1/3}Mn_{1/3}]O_2$ Cathodes for Na-Ion Battery Application. *Electrochem. Commun.* **2012**, *18*, 66−69.
(39) Carlier, D.; Cheng, J. H.; Berthelot, R.; Guignard, M.; Yoncheva, M.; Stoyanova, R.; Hwang, B. J.; Delmas, C. The P2-$Na_{2/3}Co_{2/3}Mn_{1/3}O_2$ Phase: Structure, Physical Properties and Electrochemical Behavior as Positive Electrode in Sodium Battery. *Dalton Trans.* **2011**, *40*, 9306−9312.
(40) Zhou, L.; Zhao, D.; Lou, X. $LiNi_{0.5}Mn_{1.5}O_4$ Hollow Structures as High-Performance Cathodes for Lithium-Ion Batteries. *Angew. Chem., Int. Ed. Engl.* **2012**, *51*, 239−241.
(41) Zhou, L.; Zhou, X.; Huang, X.; Liu, Z.; Zhao, D.; Yao, X.; Yu, C. Designed Synthesis of $LiMn_2O_4$ Microspheres with Adjustable Hollow Structures for Lithium-Ion Battery Applications. *J. Mater. Chem. A* **2013**, *1*, 837−842.
(42) Xiao, L.; Guo, Y.; Qu, D.; Deng, B.; Liu, H.; Tang, D. Influence of Particle Sizes and Morphologies on the Electrochemical Performances of Spinel $LiMn_2O_4$ Cathode Materials. *J. Power Sources* **2013**, *225*, 286−292.
(43) Chen, X.-F.; Qie, L.; Zhang, L.-L.; Zhang, W.-X.; Huang, Y.-H. Self-Templated Synthesis of Hollow Porous Submicron $ZnMn_2O_4$

Sphere as Anode for Lithium-Ion Batteries. *J. Alloys Compd.* **2013**, *559*, 5−10.
(44) Fei, J. B.; Cui, Y.; Yan, X. H.; Qi, W.; Yang, Y.; Wang, K. W.; He, Q.; Li, J. B. Controlled Preparation of MnO_2 Hierarchical Hollow Nanostructures and Their Application in Water Treatment. *Adv. Mater.* **2008**, *20*, 452−456.
(45) Parant, J.-P.; Olazcuaga, R.; Devalette, M.; Fouassier, C.; Hagenmuller, P. Sur Quelques Nouvelles Phases de Formule Na_xMnO_2 ($x < 1$). *J. Solid State Chem.* **1971**, *3*, 1−11.
(46) Patoux, S.; Dollé, M.; Doeff, M. M. Layered Manganese Oxide Intergrowth Electrodes for Rechargeable Lithium Batteries. 2. Substitution with Al. *Chem. Mater.* **2005**, *17*, 1044−1054.
(47) Ponrouch, A.; Marchante, E.; Courty, M.; Tarascon, J.-M.; Palacín, M. R. In Search of an Optimized Electrolyte for Na-Ion Batteries. *Energy Environ. Sci.* **2012**, *5*, 8572−8583.
(48) Ponrouch, A.; Dedryvère, R.; Monti, D.; Demet, A. E.; Ateba Mba, J. M.; Croguennec, L.; Masquelier, C.; Johansson, P.; Palacín, M. R. Towards High Energy Density Sodium Ion Batteries through Electrolyte Optimization. *Energy Environ. Sci.* **2013**, *6*, 2361−2369.
(49) Vidal-Abarca, C.; Lavela, P.; Tirado, J. L.; Chadwick, a. V.; Alfredsson, M.; Kelder, E. Improving the Cyclability of Sodium-Ion Cathodes by Selection of Electrolyte Solvent. *J. Power Sources* **2012**, *197*, 314−318.